JOURNAL OF GEOPHYSICAL RESEARCH, VOL. 101, NO. D5, PAGES 9413–9423, APRIL 27, 1996

Cross-isentropic stratosphere-troposphere exchange of mass and water vapor

Hu Yang and Ka Kit Tung

Department of Applied Mathematics, University of Washington, Seattle

Abstract. Since cross-isentropic mass fluxes are directly related to net diabatic heating, mass fluxes into the "overworld" across the 385 K and 444 K isentropes are calculated using a comprehensive radiative transfer code. Ozone, methane, water vapor, and nitrous oxide data from instruments aboard the Upper Atmospheric Research Satellite (UARS) and temperature data from United Kingdom Meteorological Office (UKMO) are used for this study. Water vapor budget for the stratosphere is calculated as an independent check on the validity of the calculated mass exchange rate. The total upward mass flux is found to be strongest in northern winter and weakest in northern summer, with an annual mean flux of 73 and 119 $\times$ 10^8 kg/s across the 444 K and 385 K isentropes, respectively, giving a turnover time of 1.6 years for the overworld.

Introduction

Mass and tracer exchanges between the stratosphere and the troposphere (STE) are important to the chemical composition of both regions. The rate of exchange affects the residence time of tracers in the stratosphere and the flux of chemically reactive species into the troposphere from the stratosphere. Therefore its determination influences greatly the assessment of ozone depletion due to the release of chlorofluorocabons (CFCs) and the impact of high-speed civil transport (HSCT) emissions.

Recently, *Holton et al.* [1995] reviewed many of the issues involved with STE, including the physical mechanisms of the exchange, previous quantitative estimates of the mass exchange rate, and STE in numerical models. They argued that for transport purposes the stratosphere should be divided into two regions: the "overworld" and extratropical "lowermost stratosphere," separated by the 380 K isentropic surface (see Figure 1). In the "overworld," global-scale meridional circulation is driven by wave-induced forces, which exert a nonlocal control over the transport of mass across lower-stratospheric isentropic surfaces as a kind of "fluid-dynamical suction pump." The transport between the lowermost stratosphere and the troposphere, on the other hand, requires the consideration of synoptic-scale processes such as penetrative cumulus convection and small-scale mixing associated with upper level fronts and cyclones. Thus exchange between the troposphere and the lowermost stratosphere can be significantly faster than exchange between the overworld and the lowermost stratosphere. *Holton et al.* [1995] argued further that for many purposes, such as for simulation of a chemical species with its chemical source or sink in the overworld, the transport across an isentrope (such as the 380 K surface) is a more relevant measure of exchange than STE across the tropopause. *Tung* [1982, 1986] previously showed that for the purpose of calculating the zonal mean transports of tracers, it is more appropriate to take zonal means of velocities along surfaces of isentropes instead of on isobars and that such isentropic means most closely approximate the Lagrangian means.

Previous studies of STE (see *Holton et al.* [1995] for references) calculated mass transport across either the tropopause (specified or estimated) or a constant pressure level (such as 100 mbar). In this paper we calculate the mass exchange rate across isentropic surfaces and compare our results with earlier estimates. Because of the uncertainties inherent in radiative transfer calculations, which are difficult to quantify, fluxes of water vapor are then used as a further check on the accuracy of the mass flux estimates.

Data and Model

A 3-year period from December 1991 to November 1994 is covered in this study. Temperature data from United Kingdom Meteorological Office (UKMO) [*Lorence et al.*, 1991; *Swinbank and O'Neil*, 1994] and tracer data from instruments aboard the Upper Atmospheric Research Satellite (UARS) [*Reber et al.*, 1993] are used. These data are archived at the Goddard Distributed Active Archive Center (DAAC) and are now publically available .

The temperature data are from UKMO data set, which is archived at the DAAC along with UARS data for the purpose of correlative studies. Ozone (retrieved from 205-GHz radiometer radiances) and water vapor

Paper number 96JD00057.
0148-0227/96/96JD-00057$05.00

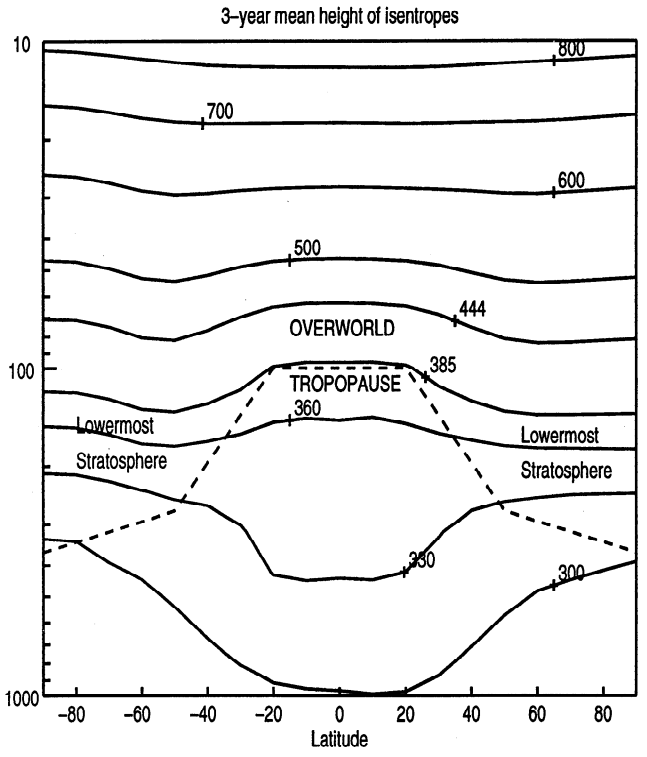

Figure 1. The mean height of isentropes during the period of December 1991 to December 1994 (solid lines). The dashed line shows a schematic tropopause.

data are from the UARS Microwave Limb Sounder (MLS) [*Barath et al.*, 1993] observation [*Waters et al.*, 1993; *Froidevaux et al.*, 1994; *Lahoz et al.*, 1996]. Methane and nitrous oxide data are from the cryogenic limb array etalon spectrometer (CLAES) observation [*Kumer et al.*, 1993]. However, MLS water vapor is available only until April 1993. The last year of MLS water vapor data from April 1992 to March 1993 is recycled in this study. CLAES methane and nitrous oxide data for the year 1992 is used for every year.

The data from DAAC have three spatial dimensions and are stored in isobaric coordinates. They should first be sorted onto isentropic surfaces and then zonally averaged before they can be used in our two-dimensional model in isentropic coordinates. For quantities such as vertical and meridional velocities, isentropic and isobaric zonal averagings often yield drastically different results. For other quantities, such as temperature and tracer mixing ratios, we find that the two zonal averages yield very similar results if the data field does not exhibit large zonal or vertical gradients. For example, UKMO temperatures calculated by the two methods are almost identical throughout the stratosphere except at high latitudes. The difference in stratosphere is generally less than 0.1 K in the tropics and middle latitudes and less than 0.5 K at high latitudes. Limited tests on UARS data show the difference in tracer mixing ratio is generally less than 1%. These errors are smaller than the uncertainties in the temperature and tracer measurements themselves. According to the ducumentations of data quality accompanied UARS data, the UKMO temperature has an estimated global average root-mean-square error of 1-2 K and local errors up to 10-20 K; the estimated error is at least 5% for MLS ozone and 15-30% for MLS water vapor.

Zonal-mean data for ozone, methane, nitrous oxide, and water vapor are from UARS 3B data sets. Zonal-mean UKMO temperature data were calculated and kindly provided to us by Eric Ray. We sort these data onto isentropic coordinates and then use them to calculate the zonal wind, radiative heating, circulation, and wave forcing. All other necessary data, including nitrogen dioxide and cloud data needed for radiative calculation, are supplied by our two-dimensional model, calculated in an isentropic coordinate system.

The tool we use for this study is our diagnostic two-dimensional model formulated in isentropic coordinates. The model has an efficient and reasonably accurate radiative transfer code [*Olaguer et al.*, 1992]. The infrared module calculates the infrared cooling due to carbon dioxide, ozone, water vapor, methane, and nitrous oxide. The solar radiation module allows for radiative absorption at ultraviolet and visible wavelengths by ozone, molecular oxygen and nitrogen dioxide, and at near-infrared wavelengths by water vapor and carbon dioxide. Three layers of clouds are assumed and latent heat release is parameterized in the troposphere. The errors in infrared heating rates under clear-sky conditions are generally within 5% or 0.05 K/d in the lower stratosphere, when compared with line-by-line calculations. The error in the net heating is, however, much larger in terms of percentage, due to the large cancelation of infrared cooling and short wave heating in the lower stratosphere.

Our model also has a fairly comprehensive photochemical package [*Yang et al.*, 1991] and self-consistent nongeostrophic formulation of dynamical transport [*Tung*, 1982, 1986; *Yang et al.*, 1990]. The model is designed as a diagnostic model and is normally constrained physically by the observed temperature as input.

In this study, our model is employed in a "data assimilation" mode. In addition to the observed temperature, UARS-observed tracer data mentioned earlier were used as inputs to our model, from which heating rates and transport parameters are calculated and chemical sources and sinks are determined for many tracer species, including O_x, NO_y, N_2O, HO_x, Cl_y, CH_4, H_2O, CO, CFCs, and HF. Then the model is integrated forward to predict ozone and other tracers five days later. If observation is available at that time, model data are replaced with observational data and the calculation proceeds. Wherever and whenever observational data are unavailable, model-assimilated data are used. The model is "initiated" every 5 days by the most recent available observational data at each grid point. This data assimilation procedure is designed to cover periodic data gaps at middle and high latitudes of about a month for each UARS yaw operation and other irregular data gaps due to operational problems. This procedure is applied to ozone, water vapor, methane, and nitrous oxide data.

Annual Mean Mass Exchange Rate

Cross-isentropic mass exchange rate can be calculated naturally by a model formulated in isentropic coordinates. As in the work of *Tung* [1982], let θ be the potential temperature, T the temperature, Q the net diabatic heating (in Kelvin degree per second), $\rho_\theta \equiv \rho\partial z/\partial \ln\theta$ and $W \equiv \rho_\theta d\ln\theta/dt$ be the density and vertical mass flow rate in isentropic coordinates, respectively. Then the thermodynamics equation

$$\frac{d}{dt}\ln\theta = \frac{Q}{T} \tag{1}$$

becomes

$$W = \rho_\theta \frac{Q}{T}. \tag{2}$$

In isentropic coordinates the cross-isentrope mass flux W is directly proportional to diabatic heating rate Q as in the above relationship, which can be used to obtain the mass flux after the diabatic heating rate Q is calculated by radiative transfer codes. Note that (2) is an exact equation with no approximation in its derivation and can be used in three-dimensional models. When it is used in a two-dimensional model where every quantity is zonally averaged, it can be approximated (as is done in this study) as

$$\bar{W} = \bar{\rho}_\theta \frac{\bar{Q}}{\bar{T}}, \tag{3}$$

where overbar denotes zonal average. The approximation involved was justified by *Tung* [1982] and *Pawson and Harwood* [1988].

We calculate $\bar{Q}$ by our radiative transfer code, using observed and, when necessary, model-assimilated data. Since temperature $\bar{T}$ is input and density $\bar{\rho}_\theta$ can be determined from $\bar{T}$, and vertical mass flux $\bar{W}$ is obtained by (3), meridional mass flux $\bar{V}$ can then be determined by employing the zonally averaged mass continuity equation

$$\frac{\partial}{\partial t}\bar{\rho}_\theta + \frac{\partial}{\partial y}\bar{V} + \frac{\partial}{\partial \ln\theta}\bar{W} = 0, \tag{4}$$

with the boundary conditions

$$\bar{V} = 0 \quad \text{at the poles.}$$

The boundary conditions are strictly enforced in our model by uniformly adjusting $\bar{W}$ on each isentropic grid level. This step corresponds to the step of subtracting the globally averaged $\bar{Q}$ from $\bar{Q}$ itself adopted by most authors using isobaric formulation. The need to adjust $\bar{W}$ or $\bar{Q}$ to satisfy mass conservation represents one of the uncertainties in calculating global transport velocities by radiative codes. It should be pointed out that the degree of imbalance in our method of calculation depends on the degree to which the data are assimilated. In the works of *Olaguer et al.* [1992] and *Yang et al.* [1991], temperature was input from National Meteorological Center (NMC) data set and the ozone and other radiatively active tracers were "assimilated" (namely, calculated) by the model. In those studies, the net radiative heating imbalance of about 0.1 K/d was found in the lower stratosphere. In the current work we use model assimilation only to supply missing data. When data are available, they are input into the radiative codes without modification. As a result, a larger and sometimes rather erratic imbalance in the net radiative heating is possible as a possible manifestation of the errors in measurements mentioned earlier.

The meridional circulation thus obtained, called diabatic circulation, should be a good representation of the actual circulation with which tracers and angular momentum are transported [*World Meteorological Organization* (WMO), 1986]. Its sense and gross patterns agree with the meridional circulation inferred by *Brewer* [1949] and *Dobson* [1956] based on the behavior of helium, water vapor, and ozone. The strength of this important circulation is, however, not a directly measured quantity and remains uncertain to this day. And that is the focus of this study.

We present results on two isentropic surfaces that are standard grid levels in our model. One of the isentropes is 385 K, which is slightly above 100 mbar in the tropical region and a little below it in the extratropics. That isentrope has a global and annual mean pressure of about 116 mbar. The other surface is the 444 K isentrope, which has a global and annual mean pressure of about 72 mbar. The mean heights of these and other isentropes averaged over a 3-year period of our study are shown in Figure 1.

The distributions of the 3-year mean area-weighted mass flux across the isentropic surfaces of 385 K and 444 K are shown in Figure 2. Upward motion is found in the tropics and subtropics. The area of ascending motion on the 385 K surface ranges from 25°S to 35°N during April–August period and from 40°S to 25°N during the remaining months. Outside this band of ascending motion, subsidence takes place, except in southern high latitudes, where it is slightly upward in and only in austral spring. The band of ascending motion on the 444 K surface in the tropics is a little wider and shifts more with season, when compared with that on the 385 K surface.

Figure 3 shows the globally integrated mass fluxes across the isentropic surfaces of 385 K and 444 K for the 3-year period from December 1991 to November 1994. Note that these mass fluxes have already been adjusted by the model to satisfy mass conservation. The top and bottom lines show the integrated upward and downward mass fluxes and the middle line shows the balance between the two. Figure 3 shows that the upward and downward mass fluxes do not exactly balance each other. On the 385 K surface, the 3-year average of global total upward mass flux is 119×10^8 kg/s and downward mass flux is 120×10^8 kg/s, leaving an average imbalance of -1×10^8 kg/s, which is less than 1%. On the 444 K surface, the corresponding numbers are 73, 74, and -1×10^8 kg/s, respectively. The net mass flows across these isentropes are due to the fact that the "overworld" has moved up higher as a result of stratospheric cooling during the 3-year period, as will be shown below.

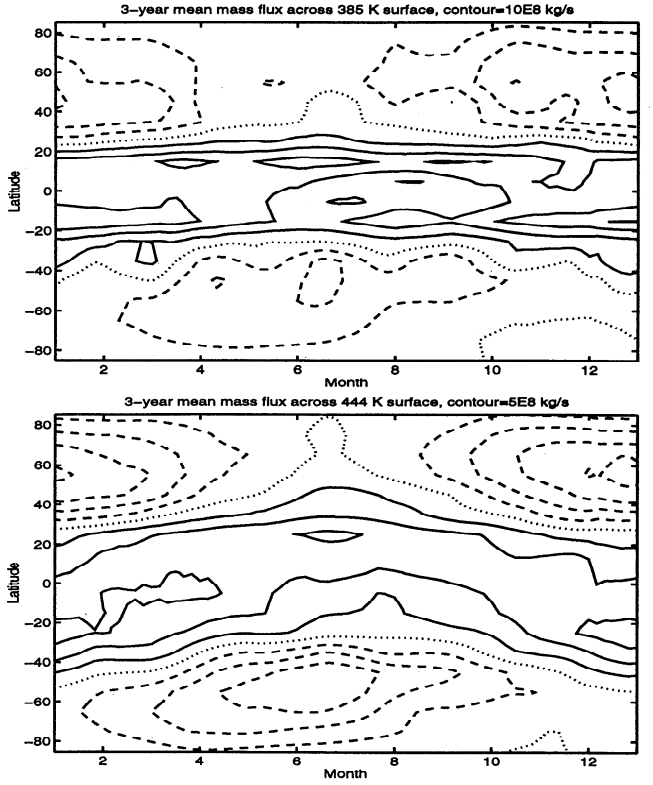

Figure 2. Distributions of the 3-year mean area-weighted mass flux across the isentropic surfaces. For the 385 K isentrope (upper panel), contour interval is 10×10^8 kg/s; for the 444 K isentrope (lower panel), contour interval is 5×10^8 kg/s. The upward fluxes are shown in solid lines, downward fluxes are shown in dashed lines, and zero in dotted lines.

Unlike in pressure coordinates, there is no requirement of instantaneous mass balance in isentropic coordinates (see equation (4)). To understand the effect of global temperature change on the mass of the stratosphere, we globally integrate (4) to get

$$< \bar{W} >= - < \frac{\partial}{\partial t} \int_{\theta}^{\inf} \bar{\rho}_{\theta} d \ln \theta' >, \qquad (5)$$

where angle brackets denote global average:

$$\frac{1}{2a} \int_{-a}^{a} < \ > dy$$

on isentropic sufaces, and the boundary conditions that $\bar{V} = 0$ at both poles and $\bar{W} = 0$ at infinity were used. Substituting

$$\bar{\rho}_{\theta} = -\frac{1}{g} \frac{\partial \bar{p}}{\partial \ln \theta}$$

into (5), we have

$$< \bar{W} >= \frac{1}{g} \frac{\partial}{\partial t} < \bar{p} >= \frac{1}{g\kappa} < \frac{\overline{p}}{T} \frac{\partial T}{\partial t} > \qquad (6)$$

since $p = p_{00}(T/\theta)^{1/\kappa}$. Equation (6) states that there is a positive global mass imbalance if isentropic surfaces move lower so that global mean pressure increases on the isentropes. On the other hand, when isentropic surfaces move higher, so that global mean pressure decreases on the isentropes, there is a negative global mass imbalance. The latter case occurs if the global mean temperature on isentropic surfaces decreases with time.

The global mean temperature, shown in Figure 4, decreased 1 K on the 385 K surface and 2 K on the 444 K surface over the 3-year period. An order of magnitude estimate of global mass imbalance can be obtained by

$$< \bar{W} > \approx \frac{1}{g\kappa} \frac{< \bar{p} >}{< \bar{T} >} \frac{\partial}{\partial t} < \bar{T} > . \qquad (7)$$

For mass imbalance on the 385 K surface over the 3-year period, $< \bar{p} >= 116$ mbar, $< \bar{T} >= 207$ K, and $< \partial \bar{T}/\partial t >= -1/3$ K per year; on the 444 K surface, $< \bar{p} >= 72$ mbar, $< \bar{T} >= 209$ K, and $< \partial \bar{T}/\partial t >= -2/3$K per year. Substituting these numbers into (7), we obtain the global mass imbalance ($< \bar{W} >$ multiplied by $4\pi a^2$, the area of the Earth's surface) of about -1×10^8 kg/s on both surfaces, as found previously.

The annual mean mass fluxes are shown schematically in Figure 5. The 3-year mean total upward mass flux is 119×10^8 kg/s across the 385 K surface and 73×10^8 kg/s across the 444 K isentrope. Therefore roughly 40% of the air crossing above the 385 K surface returns below it without crossing the 444 K surface. Since the air mass above the 385 K is about 6.0×10^{17}

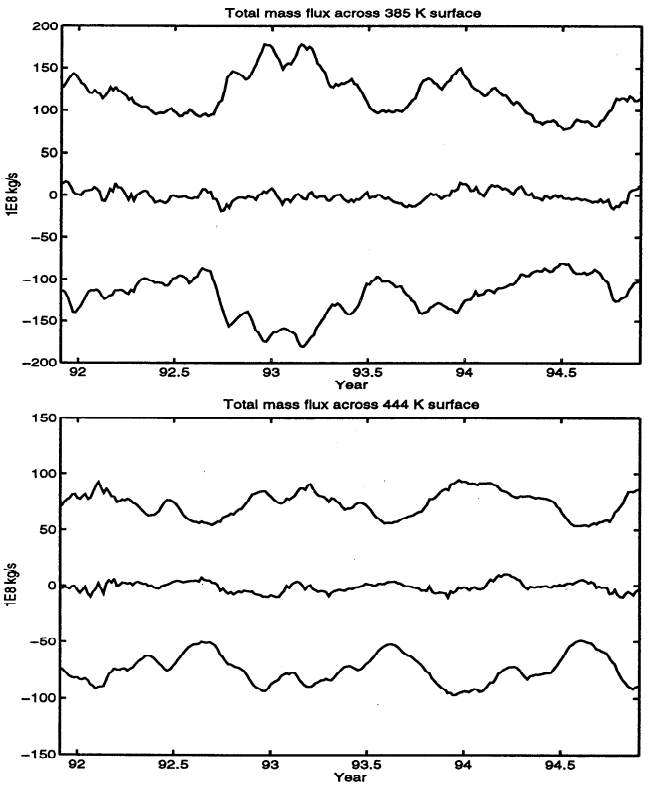

Figure 3. Globally integrated mass fluxes across the isentropic surfaces of 385 K (upper panel) and 444 K (lower panel). In each panel, the top line is total upward fluxes, the bottom line is total downward fluxes, and the middle line is the sum of the two.

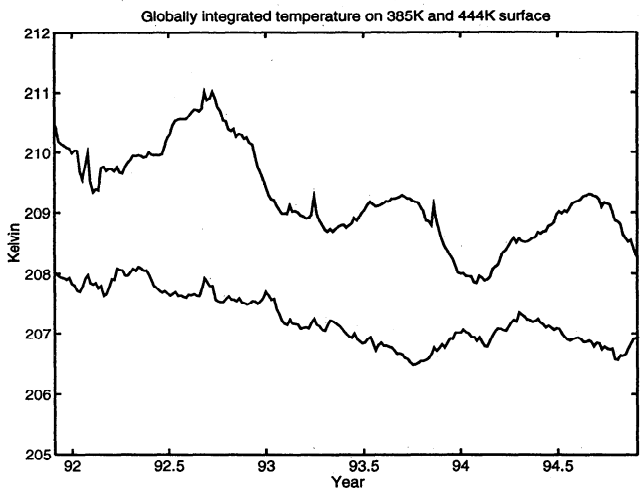

Figure 4. Global mean temperature on surfaces of 385 K (bottom line) and 444 K (top line).

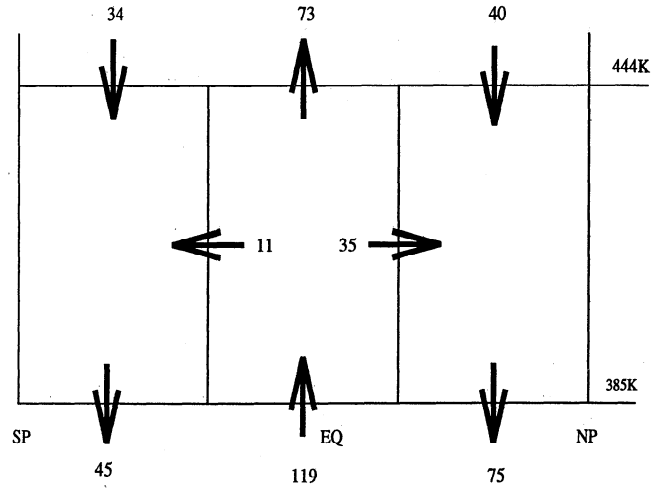

Figure 5. Schematic diagram of the annual mean mass fluxes across 385 K and 444 K isentropes.

kg and there is 3.7×10^{17} kg of air above the 444 K surface, our flux rates imply a turnover time of 1.6 years for both regions. This is shorter than some of the earlier estimates, which range from 2 to 3 years [*Holton*, 1990; *Rosenlof and Holton*, 1993; *Rosenlof*, 1995] and is closer to the turnover time of 1.7 years given by the mass fluxes calculated by *Eluszkiewicz et al.* [1996].

Our calculated 3-year mean downward fluxes crossing the 385 K surface are 75×10^8 kg/s for the northern hemisphere and 45×10^8 kg/s for the southern hemisphere. Therefore the northern hemispheric circulation is stronger than the southern hemispheric circulation by 67%, as measured by the flux crossing the 385 K surface. Much of this hemispheric asymmetry, however, is accounted for by the asymmetric poleward flow between 385 K and 444 K surfaces, so that the annual mean circulation is much more symmetric above the 444 K surface between the two hemispheres. The hemispheric difference in mass flux across the 444 K surface is less than 18%.

Our estimates for total upward (or downward) mass fluxes across the 385 K surface is roughly 50% larger than those across the 100-mbar surface calculated by *Rosenlof and Holton* [1993] and is about 24% larger than the 100-mbar fluxes calculated *Eluszkiewicz et al.* [1996]. Since 385 K surface lies below the 100-mbar surface outside the tropical region, one possible cause of discrepancy could be that part of the air crossing above the isentrope in the subtropics moves poleward and returns below the isentrope without crossing the 100-mbar isobaric surface. This effect is expected to be small however, since the vertical velocity in the subtropics is small. The errors and uncertainties associated with different methods of calculation are the other sources of discrepancy. *Rosenlof and Holton* [1993] applied the downward control principle [*Haynes et al.*, 1991] to estimate the mass flux, using UKMO data to estimate wave forcing (due to planetary wave breaking). Gravity wave drag was not included. They pointed out that it is important to include gravity wave drag in the wave forcing calculation. Using a general circulation model data, they showed that the inclusion of gravity wave forcing increased the northern hemisphere downward flux by about 10% (see *Rosenlof and Holton* [1993] for more discussion of error sources associated with their calculation). The accuracy of our method of calculation depends critically on the accuracy of radiative transfer code, which may not be better than the other methods (see *Olaguer et al.* [1992] for an assessment of the accuracy of the code and the inherent uncertainties). The input data can also be a source of discrepancies. For example, *Eluszkiewicz et al.* [1996] used the version-3 UARS MLS temperature, while we and *Rosenlof and Holton* [1993] used the UKMO temperature.

Seasonal Variation of Mass Exchange Rate

The seasonal variation of downward mass fluxes for both hemispheres are shown in Figure 6. Both hemispheres exhibit prominent seasonal cycles, the amplitude for the northern hemisphere annual cycle being the larger of the two. The seasonal variations of 3-year mean total upward and downward mass fluxes are shown in Figure 7. The seasonal mean values are also summarized in Table 1, along with the 100-mbar mass fluxes calculated by *Rosenlof and Holton* [1993] and *Eluszkiewicz et al.* [1996] for comparisons.

The global circulation, as measured by the total upward mass flux crossing 385 K surface in unit of 10^8 kg/s, is strongest in northern winter with a value of 141 units and weakest in northern summer at 97 units. The seasonal contrast, with winter value larger than the summer value by about 45%, is smaller than the contrasts reported earlier by *Holton* [1990] and *Rosenlof and Holton* [1993], who found a factor of 2 difference between northern winter and northern summer mass fluxes across the 100-mbar surface. The seasonal contrast is even smaller in our calculated downward flux (northern winter value is larger than nothern summer

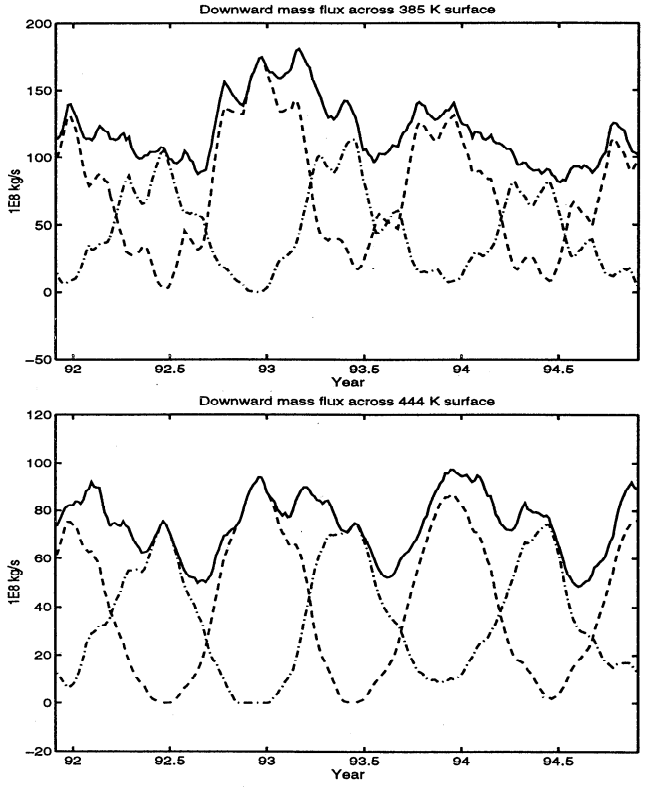

Figure 6. The magnitude of downward mass fluxes for northern hemisphere (dashed line), southern hemisphere (dashed-dotted line), and global total (solid line). The upper panel is for the 385 K isentrope and the lower panel is for the 444 K isentrope.

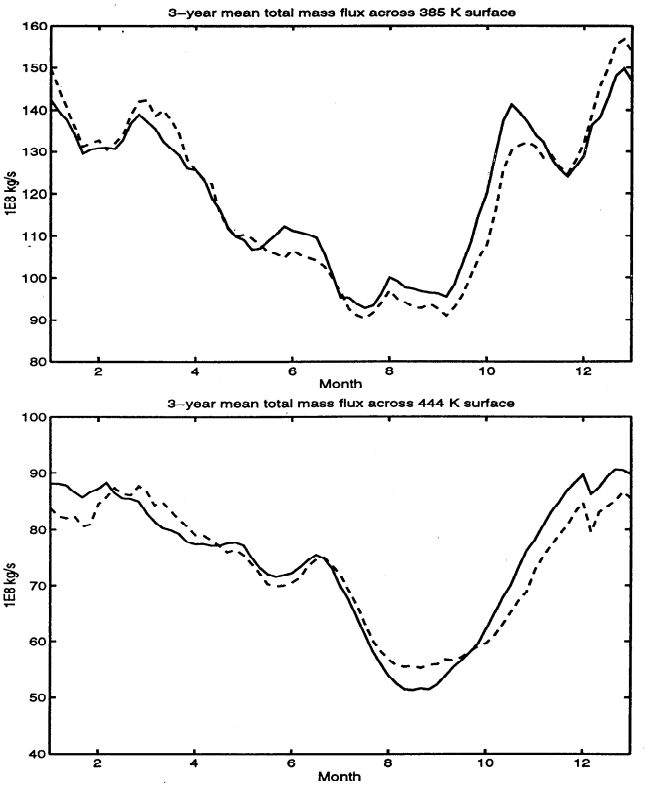

Figure 7. The seasonal variation of 3-year mean of total upward (dashed line) and downward (solid line) mass fluxes. Both fluxes are shown in positive numbers. The upper panel is for the 385 K isentrope and the lower panel is for the 444 K isentrope.

value by 37%). The seasonal contrast reported by *Eluszkiewicz et al.* [1996] is 1.7:1.

Our calculated winter hemisphere circulation is much stronger than its summer hemisphere counterpart, as one might expect from the stronger wave driving in the winter hemisphere, where planetary waves propagate upward into the westerly wind region in the stratosphere. The northern hemisphere circulation in the December–February period is stronger, by a factor of 6–7, than the southern hemisphere circulation during the same period. The contrast is smaller during southern winter, but during this period, the southern circulation is still stronger than the northern circulation by a factor of more than 2. Note that this hemispheric contrast should be smaller for the 100-mbar fluxes. Consider the thermodynamics equation in log-presure coordinates:

$$\bar{w}^* \frac{\partial \bar{\theta}}{\partial z} = \bar{Q} e^{\kappa z} - \frac{\partial \bar{\theta}}{\partial t} - \frac{\bar{v}^*}{a} \frac{\partial \bar{\theta}}{\partial \phi}, \qquad (8)$$

where $(\bar{v}^*, \bar{w}^*)$ are the transformed Eulerian mean residual velocity as defined by *Andrews et al.* [1987]. The first term on the right-hand side of (8) is the diabatic heating term; while the adiabatic terms, the second and third terms, do not appear in the isentropic formulation (3). In solstice seasons the second term on the righ-hand side of (8) is small. Since isentropes tilt upward from the summer hemisphere toward the winter hemisphere, the third term on the right-hand side of (8) is positive in the winter hemisphere and negative in the summer hemisphere in the extratropical latitudes. Therefore it serves to reduce the downward flux in the winter hemisphere and to increase the downward flux in the summer hemisphere, as compared to the values of $\bar{w}^*$ computed from $\bar{Q}$ alone. A rough estimate shows this term to be of the order of 10×10^8 kg/s in each hemisphere at solstice.

In the equinox seasons our results show also a strong hemispheric asymmetry, with the fall hemisphere circulation stronger than the one in the spring hemisphere. This result seems to be counterintuitive. However, this asymmetry should be much smaller when calculated in pressure coordinates. In spring, isentropic surfaces move lower from their annual mean positions as air is warmed by stronger sunlight. This adiabatic motion, with no cross-isentropic flux, would be counted as downward motion crossing pressure surfaces, thus enhancing the downward cross-isobaric flux in the extratropics in spring. The opposite is true in the fall hemisphere and the extratropical downward motion is reduced. This can be seen from (8) when it is applied to equinox seasons. With flat isentropes relative to pressure surface at extratropics, the third term on the righ-hand side is negligible. The second term is negative in spring as isentropes move lower relative to pressure surfaces and is positive in fall. By tracking the seasonal movement of 385 K isentropes, we estimate this effect to account

Table 1. Mass Flux Across the 385 K and 444 K Isentropic Surfaces and the 100-mbar Isobaric Surface

	444 K			385 K			100 mbar			100 mbar		
	SD	ND	UP	SD	ND	UP	SH	NH	Total	SH	NH	Total
DJF	13	74	84	18	119	141	33	81	114	14	103	117
MAM	53	24	78	72	47	121	31	46	76	60	25	85
JJA	56	7	65	68	32	97	30	26	56	64	5	69
SON	16	55	67	23	100	117	28	43	70	34	79	113
Mean	34	40	73	45	75	119	30	49	79	43	53	96

In units of 10^8 kg/s. SD and ND in column heading denote the downward fluxes in the southern and northern hemispheres, respectively. The 100-mbar fluxes on the left are taken from *Rosenlof and Holton* [1993], and the 100-mbar fluxes on the right are taken from *Eluszkiewicz et al.* [1996].

for 10-15$\times 10^8$ kg/s in each of the equinox seasons in the northern hemisphere and 15-25$\times 10^8$ kg/s in the southern hemisphere where the amplitude of annual temperature cycle is larger.

The 3-year mean seasonal variation of vertical velocities (defined here as $\bar{W}/\bar{\rho_\theta}$) across the 385 K and 444 K isentropes in the tropical region of 10°S–10°N are shown in Figure 8. On the 385 K surface the DJF mean value of 0.29 mm/s is almost twice the the JJA mean vaule of 0.16 mm/s. On the 444 K surface, late winter-early spring value of 0.5 mm/s is also about twice the (northern) summer value of 0.26 mm/s. This 2:1 seasonal contrast in tropical upwelling has been reported by *Mote et al.*, [1995, 1996], who inferred the tropical upwelling speed by tracking the movement of the total hydrogen mixing ratio in observational data. This seasonal variation in the tropical upwelling, a part of wave-driven, nonlocally controlled meridional circulation, causes the temperature in the tropical lower stratosphere to exhibit an annual cycle [*Yulaeva et al.*, 1994]. Note, however, a seasonal 2:1 contrast of tropical upwelling does not necessarily mean a 2:1 ratio in total upwelling, since the location of maximum upwelling and the area of upwelling change with season (see Figure 2).

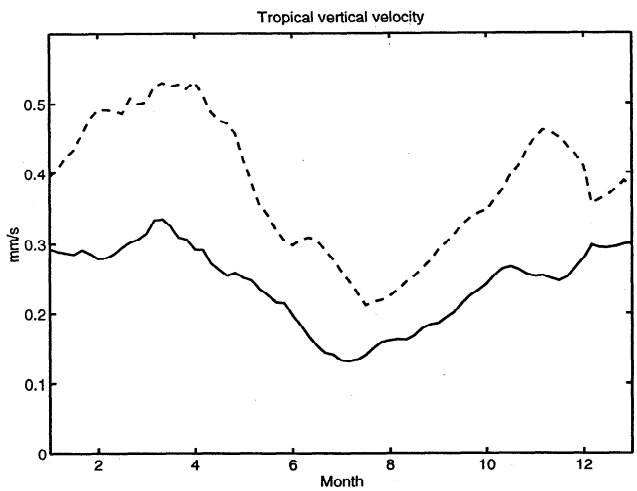

Figure 8. The 3-year mean seasonal variation of vertical velocities across the 385 K (solid line) and 444 K (dashed line) isentropes in the tropical region of 10°S–10°N.

Stratospheric Water Vapor Budget

Water vapor is an important species which plays a special role in the complex interplay of the radiative, chemical, and dynamical processes in the stratosphere. Its observed stratospheric distribution has provided much insight into the physical mechanism of STE (*Brewer* [1949]; see also *Holton* [1984] and *Holton et al.* [1995]). Here we calculate its global budget in the stratosphere, which provides a much needed independent check on the mass fluxes estimated here from radiative calculations.

Stratospheric water vapor is created through oxidation of methane, which can be written schematically as

$$CH_4 + 2O_2 \rightarrow CO_2 + 2H_2O$$

with the rate-limiting steps being

$$CH_4 + OH \rightarrow CH_3 + H_2O$$

$$CH_4 + Cl \rightarrow CH_3 + HCl$$

$$CH_4 + O(^1D) \rightarrow CH_3 + OH.$$

The actual, more extensive list of chemical reactions involving H_2O used in our model can be found in the work of *Yang et al.* [1991]. The globally integrated amount of water vapor production rate above 444 K isentrope as a function of time is shown in Figure 9. The value ranges from 1.59 to 1.76$\times 10^3$ kg/s, with a 3-year mean value of 1.68 $\times$ 10^3 kg/s.

To estimate the water vapor fluxes across the 444 K surface, we multiply the seasonal mean mass fluxes by the seasonal mean mass mixing ratio of water vapor interpolated onto the 444 K surface. The water vapor used for this purpose is based on multiyear (1986-1989) water vapor climatology observed by the Stratospheric Aerosol and Gas Experiment II (SAGE II) [*McCormick et al.*, 1993]. The results are shown in Table 2.

Our calculation shows that the water vapor has an annual mean upward flux of 1.51 $\times$ 10^4 kg/s and downward flux of 1.73 $\times$ 10^4 kg/s. There is a net downward flux of water vapor of 0.22 $\times$ 10^4 kg/s, which is mostly made up by the chemical production rate of 0.17 $\times$ 10^4 kg/s.

On a seasonal timescale, our calculation shows that

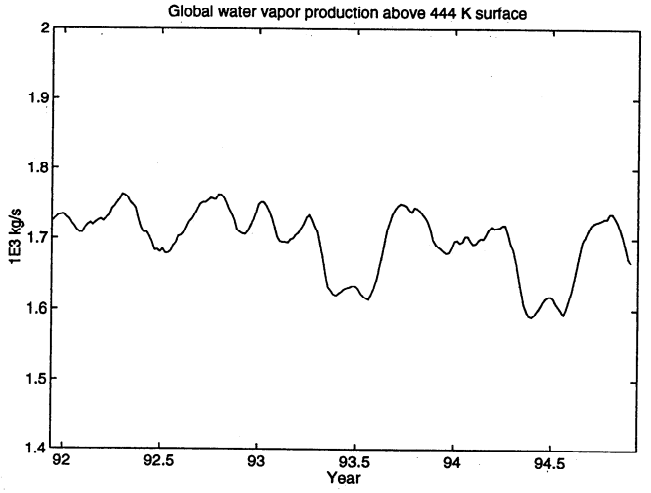

Figure 9. The globally integrated amount of water vapor production rate above the 444 K isentrope diagnosed by our photochemical model.

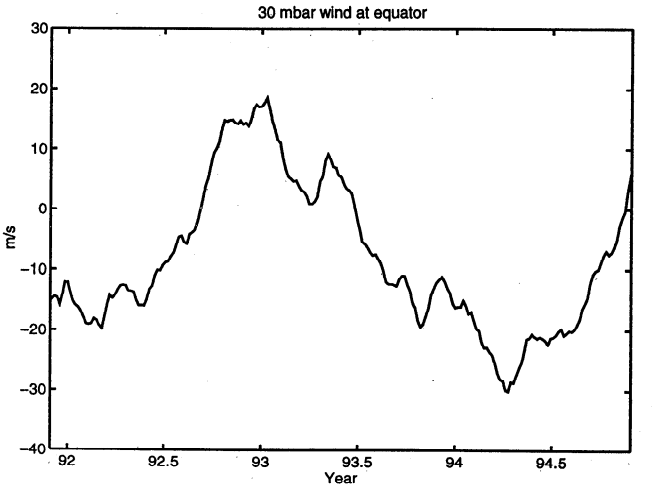

Figure 10. Zonal wind at 30 mbar at the equator calculated from United Kingdom Meteorological Office temperature by balanced wind relationship.

during the northern winter and spring, water vapor is transported out of the "overworld" at a rate larger than the chemical production rate so that a seasonal deficit exists for stratospheric water during these periods. The opposite is true during northern summer and fall months.

Interannual Variation of Circulation

In this section we present a case study of interannual variability of global circulation. Although we believe that most of the interyear variations are associated with the phenomenon of global quasi-biennial oscillation (QBO), our results can only be viewed as case studies of the two different years in opposite phases of QBO, since a 3-year period is too short for a general study of the phenomenon.

We calculate the zonally averaged zonal wind from input temperature by balanced-wind relationship, which takes the form of

$$f\bar{u} + \frac{\bar{u}^2 \tan\phi}{a} = -\frac{1}{a}\frac{\partial}{\partial\phi}\bar{\Phi}, \qquad (9)$$

where Φ is the Montgomery stream function and is related to the temperature T in isentropic coordinates as

$$\frac{\partial\bar{\Phi}}{\partial \ln\theta} = c_p\bar{T} \qquad (10)$$

Table 2. Water Vapor Flux Across the 444 K Isentropic Surface

	Up	Down	Net
DJF	1.74	2.10	-0.36
MAM	1.47	1.80	-0.33
JJA	1.33	1.42	-0.09
SON	1.49	1.60	-0.11
Mean	1.51	1.73	-0.22

In units of 10^4 kg/s.

In Figure 10 we show the calculated zonal wind near 30-mbar at the equator. The case we study here is the difference in global circulation and wave forcing between December 1992 (in the westerly phase of QBO) and December 1993 (in the easterly phase of QBO).

Figure 11 shows the distribution of the difference in vertical velocity between December 1993 and December 1992. It shows more upwelling in the lower stratosphere in the tropics and stronger downward motion in the middle and high latitudes in December 1993 than in December 1992. In other words, global circulation is stronger in December 1993 than in December 1992. In Figure 12 we show the temperature difference between the two months. The global mean temperature difference has been subtracted so that the resulted pattern is more relevant to transport. Figure 12 shows that the monthly mean temperature in the tropical lower stratosphere is lower by up to 5°K in December 1993 than

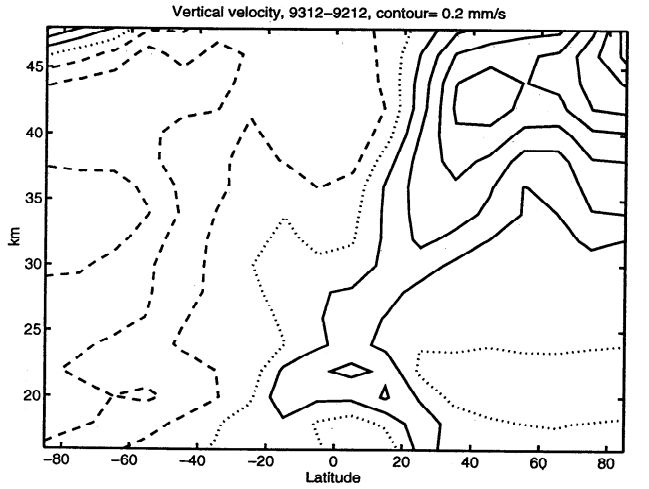

Figure 11. Distribution of the difference in vertical velocity between December 1993 and December 1992. The positive numbers are shown in solid lines, negative numbers are shown in dashed lines, and zero in dotted lines. Contour interval is 0.2 mm/s.

in December 1992 and is higher by up to 7°K in the high northern latitudes. This global pattern of temperature change is probably due to the increased heat transport from tropics to high latitudes in the easterly phase of QBO compared to the case in the westerly phase of QBO. Note that the quadrupole pattern of the temperature anomaly shown in Figure 12 is very similar to the model-calculated result in Figure 2 of *Tung and Yang* [1994], in which the temperature response to an assumed simple extratropical QBO wave forcing is shown. *Randel* [1993] also found such a pattern as characteristic of the observed large-scale transient events in the stratosphere.

Since the meridional circulation in the overworld is driven by waves and eddies, interannual variations in the circulation implies corresponding changes in wave forcing. The E-P flux (pseudo) divergence $\Box \cdot F$ can be diagnosed by the following momentum budget [*Tung*, 1986]:

$$\bar{\rho}_\theta \frac{\partial}{\partial t}\bar{L} + \bar{V}\frac{\partial}{\partial y}\bar{L} + \bar{W}\frac{\partial}{\partial \ln\theta}\bar{L} = \Box \cdot F, \qquad (11)$$

where $L = (u + \Omega a \cos\phi)\cos\phi$ is the absolute angular momentum divided by a in the zonal direction. Figure 13 shows the difference and average in E-P flux divergence between December 1993 (with QBO in easterly phase) and December 1992 (with QBO in westerly phase). The wave forcing is stronger during QBO easterly phase due to enhanced wave breaking in the narrower westerly waveguide squeezed by the easterly wind [*Holton and Tan*, 1980; *McIntyre*, 1982]. The difference is found to be about $1\text{–}2\times10^{-5}$ m/s^2 in the northern middle latitude in the lower to middle stratosphere, which is about half the magnitude of the background value of E-P flux divergence there. Although the difference can contain other interannual variability, to attribute a major part of it to QBO variation is consistent

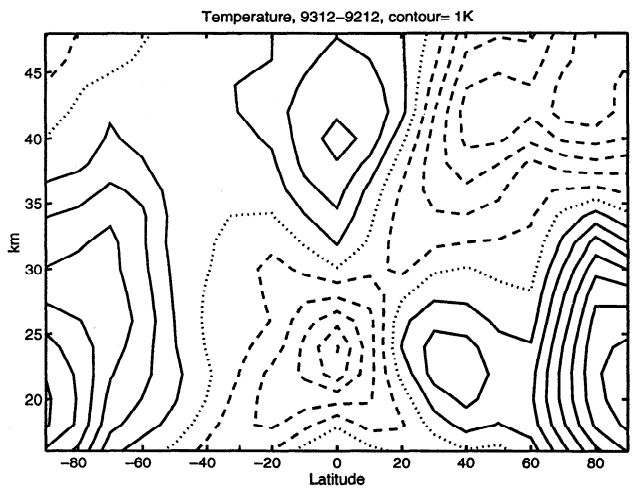

Figure 12. Distribution of the temperature difference between December 1993 and December 1992. The global mean temperature difference has been subtracted. The positive numbers are shown in solid lines, negative numbers are shown in dashed lines, and zero in dotted lines. Contour interval is 1K.

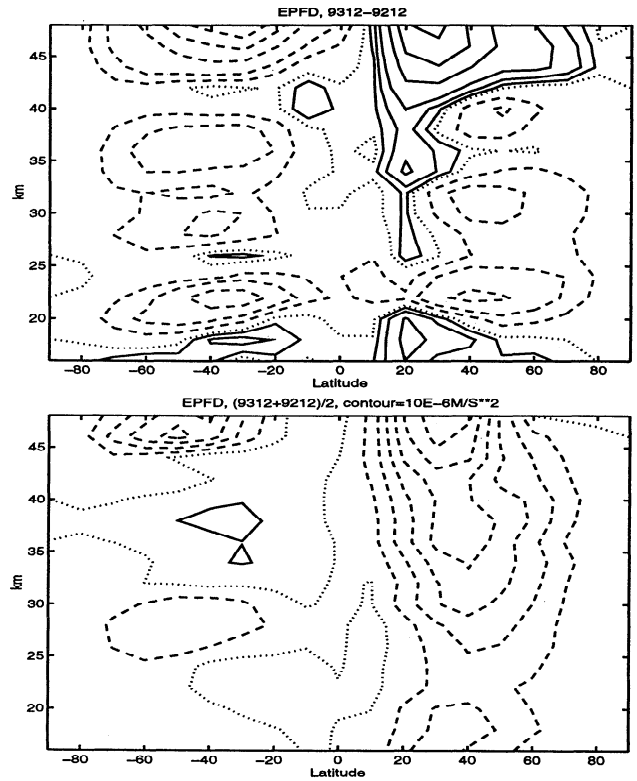

Figure 13. Distribution of E-P flux divergence for the months of December 1993 and December 1992. Upper panel shows the difference between the two months with the contours shown at irregular intervals at levels of 0, 0.2, $\pm0.5, \pm1, \pm2, \pm3, \pm4 \times10^{-5}$ m/s^2; lower panel shows the average for the two months with regular contour interval of 1×10^{-5} m/s^2. The positive numbers are shown in solid lines, negative numbers are shown in dashed lines, and zero in dotted lines.

with the findings of *Dunkerton and Baldwin* [1991]. The dipole structure in the QBO-induced change in E-P flux divergence found by *Dunkerton and Baldwin* [1991] is also present here. The existence of a QBO-related wave forcing in the middle and upper stratosphere which is consistent with the interannual variation in the strength of tropical upwelling is further evidence of nonlocal control of meridional circulation in the overworld.

Summary and Conclusions

The mass exchange rates across isentropic surfaces are calculated using the diabatic circulation diagnosed from UARS and UKMO data. Upward flux is found in the tropical and subtropical regions and downward flux is generally found in high latitudes. The total upward mass flux is strongest in northern winter and weakest in northern summer, with an annual mean flux of 73 and 119×10^8 kg/s across the 444 K and 385 K isentropes, respectively, giving a turnover time of 1.6 years for the overworld. Cross-isentropic mass flux exhibits different seasonal and hemispheric variations than its isobaric counterpart, and the reasons for this difference are discussed. In particular, we find that the 385 K total mass

flux is only about 40% larger in northern winter than in northern summer. The stratosphere-troposphere exchange also exhibits interannual variations possibly associated with the phenomenon of QBO.

The meridional circulation obtained in this study is based on diabatic heating rates calculated by a radiative transfer code. One can estimate the wave forcing using this circulation as is done in this and other previous studies. The wave forcing can also be estimated directly using large-scale eddy statistics, as is done by *Holton* [1990]. Once the wave forcing is determined, one can calculate the meridional circulation based on "downward-control" principle [*Haynes et al.*, 1991]. *Rosenlof* [1995] showed that the two approaches yield consistent results.

Since the diabatic heating rates are computed as small differences between large contributions of opposite sign, radiatively derived meridional circulation remains uncertain, especially in the lower stratosphere where the net heating rate is very small. Wave forcing calculation based on large-scale eddy statistics is also by no means certain. An independent way to determine the strength of STE is by considering the budget of tracer species in the atmosphere. *Follows* [1992] used $CFCl_3$ budget to estimate the mass flux to be about $160 \pm 60 \times 10^8$ kg/s across the 100-mbar surface. Our estimate is at the low end of his calculated range.

In this study we also calculated the global water vapor budget in the stratosphere as a check on our mass flux calculations. Using Sage II water vapor distribution in the lower stratosphere, we calculated that the water vapor has an annual mean upward flux of 1.51×10^4 kg/s and downward flux of 1.73×10^4 kg/s across the 444 K isentrope. The net downward flux of 0.22×10^4 kg/s agrees quite well with our estimated chemical production rate of 0.17×10^4 kg/s, giving us somewhat more confidence in the mass flux calculations.

Acknowledgments. We would like to thank J. R. Holton, J. Eluszkiewicz, and K. H. Rosenlof for their helpful comments and suggestions. We are grateful to Eric Ray, who supplied the zonal-mean temperature data used in this study. Science data provided by the EOS Distributed Active Archive Center (DAAC) at NASA/Goddard Space Flight Center are also used. The research is supported by NASA, under grants NAG-1-1404 and NAG 5-2802.

References

Andrews, D. G., J. R. Holton, and C. B. Leovy, *Middle Atmospheric Dynamics*, 489 pp., Academic, Orlando, Florida, 1987.

Barath, F. T., M. C. Chavez, R. E. Cofield, et al., The Upper Atmosphere Research Satellite microwave limb sounder instrument, *J. Geophys. Res., 98*, 10,751-10,762, 1993.

Brewer, A. W., Evidence for a world circulation provided by the measurement of helium and water vapour distribution in the stratosphere, *Quant. J. R. Meteorol. Soc., 75*, 351-363, 1949.

Dobson, G. M. B., Origin and distribution of polyatomic molecules in the atmosphere, *Proc. R. Soc. London, A236*, 187-193, 1956.

Dunkerton, T. J., and M. P. Baldwin, Quasi-biennial modulation of planetary-wave fluxes in the northern hemispheric winter, *J. Atmos. Sci., 48*, 1043–1061, 1991.

Eluszkiewicz, J., D. Crisp, R. Zurek, L. Elson, E. Fishbein, L. Froidevaux, J. Waters, R. G. Grainger, A. Lambert, R. Harwood, and G. Peckham, Residual circulation in the stratosphere and lower mesosphere as diagnosed from Microwave Limb Sounder data, *J. Atmos. Sci., 53*, 217-240, 1996.

Follows, M. J., On the cross-tropopause exchange of air, *J. Atmos. Sci., 49*, 879-882, 1992.

Froidevaux, L., J. W. Waters, W. G. Read, L. S. Elson, D. A. Flower, and R. F. Jarnot, Global ozone observations from UARS MLS: An overview of zonal mean results, *J. Atmos. Sci., 51*, 2846-2866, 1994,

Haynes, P. H., C. J. Marks, M. E. McIntyre, T. G. Shepherd, and K. P. Shine, On the "downward control" principle for extratropical diabatic circulations, *J. Atmos. Sci., 48*, 651-678, 1991.

Holton, J. R., Troposphere-stratosphere exchange of trace constituents: The water vapor puzzle, in *Dynamics of the Middle Atmosphere*, edited by J. R. Holton and T. Matsuno, pp. 369-385, Terrapub, Tokyo, 1984.

Holton, J. R., On the global exchange of mass between the stratosphere and troposphere, *J. Atmos. Sci., 47*, 392-395, 1990.

Holton, J. R., and H. C. Tan, The influence of the equatorial quasi-biennial oscillation on the global circulation at 50 mb, *J. Atmos. Sci., 37*, 2200–2208, 1980.

Holton, J. R., P. H. Haynes, M. E. McIntyre, A. R. Douglass, R. B. Rood, and L. Pfister, Stratosphere-troposphere exchange, *Rev. Geophy., 33*, 403-439, 1995.

Kumer, J. B., J. L. Mergenthaler, and A. E. Roche, CLAES CH_4, N_2O and CCl_2F_2 (F12) global data, *Geophys. Res. Lett., 20*, 1239-1242, 1993.

Lahoz, W. A., et al., Validation of UARS microwave limb sounder 183-GHz H_2O measurements, *J. Geophys. Res.*, in press, 1996.

Lorence, A. C., R. S. Bell, and B. Macpherson, The Meteorological Office analysis correction data assimilation scheme, *Q. J. R. Meteorol. Soc., 117*, 59-89, 1991.

McCormick, M. P., E. W. Chiou, L. R. McMaster, W.P. Chu, J. C. Larsen, D. Rind, and S. Oltmans, Annual variations of water vapor in the stratosphere and upper troposphere observed by the Stratospheric Aerosol and Gas Experiment II, *J. Geophys. Res., 98*, 4867-4874, 1993.

McIntyre, M. E., How well do we understand the dynamics of stratospheric warming? *J. Meteorol. Soc. Jpn., 60*, 37-65, 1982.

Mote, P. W., K. H. Rosenlof, J. R. Holton, R. S. Harwood, and J. W. Waters, Seasonal variations of water vapour in the tropical lower stratosphere, *Geophys. Res. Lett., 22*, 1093-1096, 1995.

Mote, P. W., K. H. Rosenlof, M. E. McIntyre, E. S. Carr, J. C. Gille, J. R. Holton, J. S. Kinnersley, H. C. Pumphrey, J. M. Russell III, and J. W. Waters, An atmospheric tape-recorder: The imprint of tropical tropopause temperatures on stratospheric water vapor, *J. Geophys. Res., 101*, 3989-4006, 1996.

Olaguer, E. P., H. Yang, and K. K. Tung, A reexamination of the radiative balance of the stratosphere, *J. Atmos. Sci., 49*, 1242-1263, 1992.

Pawson, S., and R. S. Harwood, Monthly-mean diabatic circulations in the stratosphere, *Quart. J. R. Meteorol. Soc., 115*, 807-840, 1988.

Randel, W. J., Global variations of zonal-mean ozone during stratospheric warming events, *J. Atmos. Sci. 50*, 3308-3321, 1993.

Reber, C. A., C. C. Trevathan, R. J. McNeal, and M.

R. Luther, The Upper Atmosphere Research Satellite (UARS) mission, *J. Geophys. Res., 98,* 10,643-10,647, 1993.

Rosenlof, K. H., The seasonal cycle of the residual mean meridional circulation in the stratosphere, *J. Geophys. Res., 100,* 5173-5191, 1995.

Rosenlof, K. H., and J. R. Holton, Estimates of the stratospheric residual circulation using the downward control principle, *J. Geophys. Res., 98,* 10,465-10,179, 1993.

Swinbank, R., and A. O'Neill, A stratosphere-troposphere data assimilation system, *Mon. Weather Rev., 122,* 686-702, 1994.

Tung, K. K., On the two-dimensional transport of stratospheric trace gases in isentropic coordinates, *J. Atmos. Sci., 39,* 2230–2355, 1982.

Tung, K.K., Nongeostrophic theory of zonally averaged circulation, I, Formulation, *J. Atmos. Sci., 43,* 2600–2618, 1986.

Tung, K. K., and H. Yang, Global QBO in circulation and ozone, II, A simple mechanistic model, *J. Atmos. Sci., 51,* 2708–2721, 1994.

Waters, J. W., L. Froidevaux, W. G. Read, G. L. Manney, L.S. Elson, D. A. Flower, R. F. Jarnot, and R. S. Harwood, Stratospheric ClO and ozone from the Microwave Limb Sounder on the Upper Atmosphere Research Satellite, *Nature, 362,* 597-602, 1993.

World Meteorological Organization (WMO), Atmospheric ozone 1985: Assessment of our understanding of processes controlling its present distribution and change, *WMO Rep. 16,* Global Ozone Res. and Monit. Proj., Geneva, 1986.

Yang, H., K. K. Tung, and E. P. Olaguer, Nongeostrophic theory of zonally averaged circulation, II, Eliassen-Palm flux divergence and isentropic mixing coefficient, *J. Atmos. Sci., 47,* 215–241, 1990.

Yang, H., E. Olaguer, and K. K. Tung, Simulation of the present-day atmospheric ozone, odd nitrogen, chlorine and other species using a coupled 2-D model in isentropic coordinates, *J. Atmos. Sci., 48,* 442-471, 1991.

Yulaeva, E., J. R. Holton, and J. M. Walace, On the cause of the annual cycle in the tropical lower stratospheric temperature, *J. Atmos. Sci., 51,* 169-174, 1994.

K. K. Tung and H. Yang, Department of Applied Mathematics, University of Washington, Box 352420, Seattle, WA 98195-2420. (email: tung@amath.washington.edu; yang@amath.washington.edu)

(Received August 8, 1995; revised November 16, 1995; accepted November 16, 1995.)